Available online at www.sciencedirect.com

ScienceDirect

Procedia Computer Science 239 (2024) 2135–2141

Procedia Computer Science

www.elsevier.com/locate/procedia

CENTERIS – International Conference on ENTERprise Information Systems / ProjMAN – International Conference on Project MANagement / HCist – International Conference on Health and Social Care Information Systems and Technologies 2023

Along-Track Displacement of Mw 7.8 and 7.6 Kahramanmaraş Earthquakes from Sentinel-1 Offset Tracking and Burst Overlap Interferometry

Muhammet Nergizci*, Milan Lazecky, Qi Ou, Tim Wright, Andrew Hooper

COMET, School of Earth and Environment, University of Leeds, Leeds LS29JT, UK

Abstract

On 6th February, a pair of significant earthquakes with magnitudes of 7.8 and 7.6 struck Kahramanmaraş, Turkey. The Earthquake InSAR Data Provider (EIDP) promptly produced interferograms and offset tracking results within 3 hours of acquiring Sentinel-1 satellite data. However, it was challenging to unwrap the interferograms correctly due to high displacement gradient near the rupture. Hence, early displacement fields were derived from Pixel Offset Tracking (POT) method both in range and azimuth direction with low resolution depending on pixel sizes of Sentinel-1. We used the Burst Overlap Interferometry (BOI) method to extract the accurate along-track displacement and unwrapped the BOI interferogram using Azimuth Offset Tracking (AOT) data as a guide. Combining the unwrapped BOI interferogram and the AOT data, we derive a high-quality along-track displacement field that illuminates the entire earthquake rupture over 300 km and exhibits ±4 m displacement in the along-track direction.

Keywords: Along-Track Displacement; Azimuth Offset Tracking; Burst Overlap Interferometry; Kahramanmaraş Earthquakes.

* Corresponding author.
E-mail address: eemne@leeds.ac.uk

1877-0509 © 2024 The Authors. Published by Elsevier B.V.

10.1016/j.procs.2024.06.401

1. Introduction

On 6th February 2023, Turkey experienced two devastating earthquakes within 10 hours. The hypocenter of the first 7.8 Mw event was Nurdaği in Gaziantep province at a depth of 17.9 km, while the hypocenter of the second earthquake, measuring 7.6 Mw, was Ekinözü in the Kahramanmaraş province at a depth of 10 km, approximately 100 km north of the epicenter of the first earthquake. The confirmed total number of fatalities from the earthquakes was over 50,000, and 120,000 citizens were injured in Turkey within 10 cities around the earthquakes' epicenters. Additionally, the death toll reached 8,000 in Syria. With such a high number of casualties, this event stands as the deadliest natural disaster in modern Turkish history. Regarding the deformation caused by the earthquakes, geodetic measurements indicated that the 7.8 Mw earthquake resulted in a 300 km fault rupture on the East Anatolian Fault (EAF). Additionally, the second magnitude 7.6 earthquake generated a 150 km rupture zone on the Çardak and Doğanşehir faults [1].

The magnitude of the earthquakes and the extensive fault ruptures present challenges for standard interferograms in detecting the total displacement and tracking surface ruptures in near fields. In such cases, Pixel Offset Tracking (POT) is a common method based on amplitude information rather than the phase component to extract both range and azimuth displacement from radar images [2], [3]. The principle of POT method is to track subpixel amplitude information and find offsets in range and azimuth by applying cross-correlation technique [4]. Furthermore, Split-bandwidth interferometry, which exploits Spectral Diversity (SD), is another common method to estimate deformations in both azimuth and range directions [5]. The method splits the raw SAR signal into upper and lower spectral sub-bands and then applies double difference interferogram to estimate 2D displacements, also referred to as Multiple Aperture Interferometry (MAI) [6].

Moreover, Grandin (2016) proposed Burst Overlap Interferometry (BOI) to employ burst overlap region in Sentinel-1 TOPS mode since burst overlaps already have two acquisitions with different geometries, backward- and forward-looking due to the squint angle in the azimuth direction (1°); this leads to a larger spectral separation in burst overlaps, compared to spectral separation of synthetic lower and upper sub-bands in MAI method [7]. Previous studies show that this advantage of Sentinel-1 TOPS mode supplies remarkable accuracy in azimuth displacement compared to MAI and POT methods [8]–[10], but the overlap areas only correspond to ±10% of the whole frame. The method is originally employed to coregister secondary images to a primary image in TOPS processing as called Enhanced Spectral Diversity (ESD) [7].

Regarding BOI, if the phase difference between neighboring pixels exceeds the ambiguity band, the phase difference becomes wrapped, leading to an aliased estimate. In such cases, the BOI technique requires an unwrapping process. However, due to the intervals between each burst overlap (±17 km), the unwrapping step becomes challenging using conventional 2D methods like SNAPHU [11]. Therefore, in this paper, we utilize the azimuth offset tracking result to guide the unwrapping process for BOI.

The paper is structured as follows. The second section provides a brief introduction to the Earthquake InSAR Data Provider (EIDP) and its role in monitoring Turkey's earthquakes. Additionally, the section compares the results obtained from interferograms and offset tracking provided by EIDP. The third section discusses a novel unwrapping method for BOI, which utilizes azimuth offset tracking as a guide. Furthermore, the section presents a comparison between the final unwrapped BOI results and those obtained from Pixel Offset Tracking.

2. InSAR data of the Kahramanmaraş Earthquake

EIDP operated by the Centre for the Observation and Modelling of Earthquakes, Volcanoes, and Tectonics (COMET), generated the interferograms for the event within 3 hours of the first acquisition by the Sentinel-1 satellite after the earthquakes [12]. EIDP utilizes the Looking into the Continents from Space with Synthetic Aperture Radar (LiCSAR) infrastructure to generate co-seismic interferometric pairs in an automated and rapid manner during an earthquake event. It also produces pre- and post-seismic interferograms and publishes these datasets on the COMET LiCS portal. These datasets are made widely and freely available for everyone [13].

When a minimum 5.5 Mw earthquake occurs in a continental area worldwide, the Earthquake InSAR Data Provider (EIDP) is triggered to initiate the framing of the potentially affected regions by the earthquake. Subsequently, the standard LiCSAR process begins generating the required interferograms [12]. LiCSAR utilizes the European

Commission's Copernicus Sentinel-1 A/B constellation, which operates in the C-band of the electromagnetic spectrum. While the Sentinel-1 A satellite, launched in April 2014, is still operational and captures images, the Sentinel-1 B satellite, which commenced its mission two years later, experienced a failure on 23 December 2021 and is no longer operational. The resulting products were made available on the LiCS portal, which can be accessed at the following link: https://comet.nerc.ac.uk/earthquakes/us6000jllz.html. As seen in Fig. 1a, the conventional interferogram generated from Sentinel-1 exhibits phase aliasing and complete decorrelation in the near-fault field. These issues arise due to the presence of a high displacement gradient in that area.

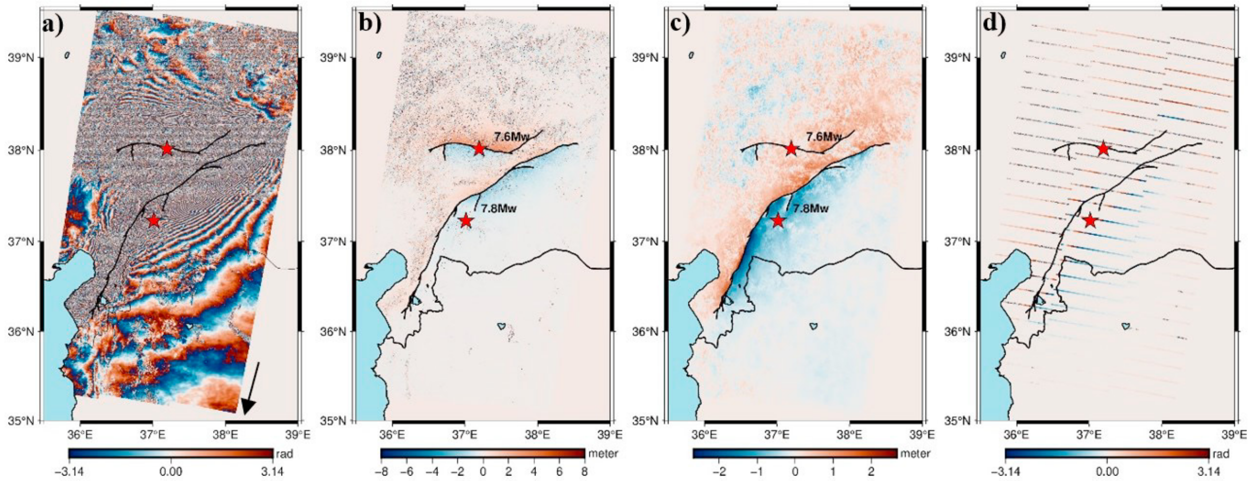

Fig.1. EIDP response to Kahramanmaras Earthquakes. The Sentinel-1 data acquired 29/01/2023 and 10/02/2023, before and after the earthquakes. The frame ID is 021D_05266_252525 in the LiCS portal. **(a)** Standard Interferogram, the black arrow shows the flight direction, red stars are the earthquakes' epicenters, and bold black lines indicate the faults, **(b)** Range offset tracking, **(c)** Azimuth offset Tracking, and **(d)** Burst overlap Interferogram.

This problem of phase aliasing and decorrelation poses challenges for accurate phase unwrapping, making it difficult to identify fault traces and determine deformation values in the near field. In the literature, Pixel Offset Tracking (POT) is commonly referred to extract unambiguous ground displacements in areas with large deformations, such as fault ruptures and volcanic craters [4], [14], [15]. It is also exploited as auxiliary information to unwrap standard interferograms [9], [16].

To overcome the same issue for Turkey earthquakes, EIDP incorporates pixel offset tracking that generates results of lower sensitivity to displacements yet capturing the high deformation gradient of such strong co-seismic signal, see Fig. 1b, c for outputs of range and azimuth pixel offsets. For the POT, we searched for azimuth/range offsets using 128/64 windows spaced by 40/16 pixels, respectively, in oversampled previously deramped mosaics of Sentinel-1 TOPS data. We select offsets with cross-correlation coefficient over 0.1 and spatially filter resulting offsets using median filter. BOI was also generated for the earthquakes to obtain more sensitive measurements in the azimuth direction, as shown in Fig. 1d.

3. Unwrapping Burst Overlap Interferogram through Azimuth Offset Tracking

In TOPS (Terrain Observation by Progressive Scans) mode, the squint angle from backward to forward in the along-track direction creates two distinct viewing geometries. The BOI method utilizes the inherent spectral diversity in the burst overlap regions to produce the double difference interferogram, Φ_{ovl}, as

$$\Phi_{ovl} = (r_{i+1} \cdot s_{i+1}^{*}) \cdot (r_i \cdot s_i^{*})^{*} \tag{1}$$

where ***r*** and ***s*** denote the primary and secondary complex images, indices ***i*** and ***i+1*** the backward- and forward-looking views, respectively, and the asterisk indicates conjugate multiplication. Scheiber and Moreira (2000) showed that phase differences derived from double-difference interferogram give along-track displacement as

$$\Delta\phi_{ovl} = 2\pi \cdot \Delta f_{ovl} \cdot \frac{\Delta x_{az}}{\Delta x_s} \cdot \Delta t_s \tag{2}$$

where Δf_{ovl} is spectral separation (~4300 Hz) within burst overlap areas in TOPS mode, Δx_s is azimuth pixel size (~14 m), Δt_s denotes azimuth sampling (~0.002 s) and Δx_{az} is azimuth displacement. In BOI, thus, a complete cycle of phase ($2\boldsymbol{\pi}$ radians or 1 "fringe") is caused by ~150 cm of azimuth displacement. Consequently, an unwrapping process becomes necessary when dealing with deformations that exhibit a very large displacement. Fig. 1.d illustrates the wrapped BOI signal for the Turkey Earthquakes, indicating that the phase needs to be unwrapped to accurately determine the true phase differences across the interferogram. Performing a standard unwrapping algorithm within each burst overlap area and dealing with the empty area between burst overlaps is challenging because of the narrow strip of data available and because of areas of noise. To our knowledge, there is no study in the literature that addresses the unwrapping issue of BOI.

In this study, we use the low-resolution AOT as a guide to help unwrapping the BOI (Fig. 2). Firstly, we convert the unit of the azimuth offset from meters to radians using Eq. 2. Then, we unwrap the BOI by adding the wrapped difference between the BOI and the azimuth offset to the azimuth offset. The unwrapped BOI would be correct if the error in the azimuth offset is within the range of - π to **π.** If the azimuth offset was wrong by more than ± π, an unwrapping error would occur. To address this issue, we look for discontinuities that are present in the unwrapped BOI but not in the wrapped BOI and correct the error by adding or subtracting multiples of $2\boldsymbol{\pi}$ from the affected region. By following the flowchart outlined in Fig. 2, the unwrapped BOI for Turkey earthquakes is obtained. The resulting unwrapped BOI clearly reveals the fault traces of the East Anatolian Fault (EAF) and indicates significant left-lateral displacement reaching ±4 meters in along-track direction (Fig. 3). Furthermore, it is evident that the BOI is influenced by decorrelated areas such as regions with dense vegetation, forests, lakes, and areas with significant displacement gradients in the near field. Consequently, these areas may appear as noisy pixels in the BOI rather than providing reliable phase information, similar to the standard InSAR observations. To tackle this issue, BOI is filtered using adaptive filtering during the production step in LiCSAR with the "adf" command in GAMMA software [17].

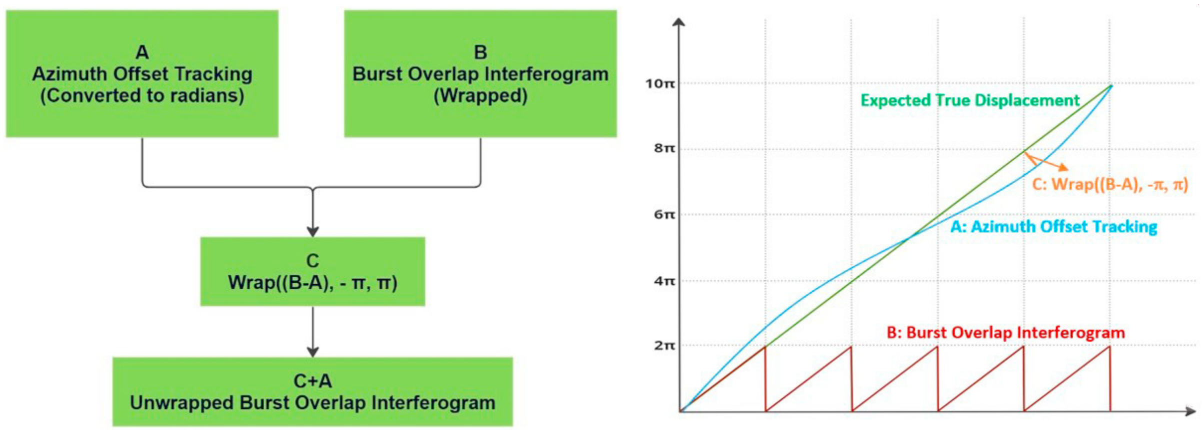

Fig. 2. Flowchart of Unwrapping BOI with Azimuth Offset. The units of the input and output are the radian (Left). Illustration of simplified AOT and BOI regarding to expected surface displacement (Right).

While the unwrapping process is successfully carried out, it is important to note that the BOI method is applicable only within the burst overlap areas, which account for approximately 10% of the entire frame. To address the empty

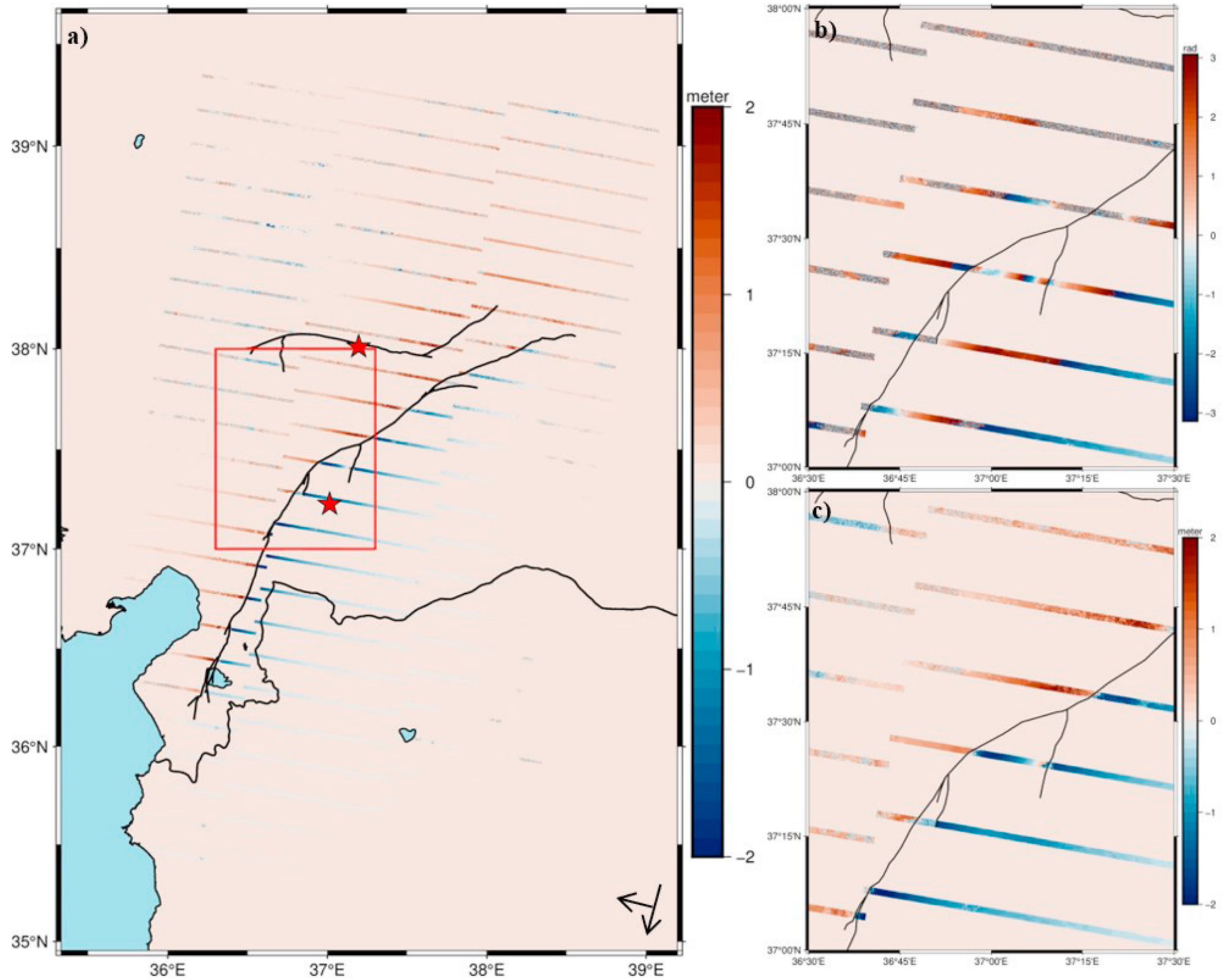

Fig. 3. Comparison of BOI before and after unwrapping. **(a)** The whole unwrapped frame of BOI. Red rectangular represent the zoomed area to see the comparison in detail. The black arrow shows the flight direction. **(b)** The wrapped BOI with the radian unit, **(c)** the unwrapped BOI with the meter unit.

areas outside the burst overlaps, we utilize AOT to capture the overall trend of displacement. However, it is worth mentioning that the AOT has lower accuracy compared to BOI (Fig. 4). By combining the BOI and AOT results, we can obtain a more comprehensive representation of the displacement field, considering both the high accuracy of BOI within the burst overlap areas and the general trend provided by AOT. In Fig. 4, the sensitivity of BOI is clearly demonstrated, resulting in distinct burst overlaps compared to the blurred AOT pixels that encompass them.

The cross-section analysis also depicts the response of both methods to a significant displacement gradient present along the fault (Fig. 4b). The AOT method demonstrates a gradual and smooth change along the profile, including a gradual transition over the fault area. On the other hand, the BOI method exhibits a sharper and more sudden change over the fault, emphasizing its ability to capture and depict abrupt displacement gradients. In addition, BOI cross-section shows a fluctuation near the fault because of the unwrapping error and low decorrelation around the fault. This noise can be removed by applying a filtering or removing/adding 2π.

4. Conclusion

Standard InSAR may not be effective in extracting displacement and fault trace information in a large-magnitude earthquake event with a significant displacement gradient. Furthermore, standard InSAR techniques provide displacement information only in the Line-of-Sight (LOS) direction. Although Pixel Offset Tracking (POT) and Multiple Aperture Interferometry (MAI) can extract displacement information in both the azimuth and range directions their measurement accuracy is limited by the azimuth pixel size and effective bandwidth, respectively. On the other hand, Burst Overlap Interferometry (BOI) can provide high-quality and high-resolution displacement measurements in the along-track direction at pixels in the burst overlaps. We develop a method for unwrapping of the BOI data using the azimuth offset data as a guide and produce the highest quality along-track displacement field for the 2023 Turkey earthquakes.

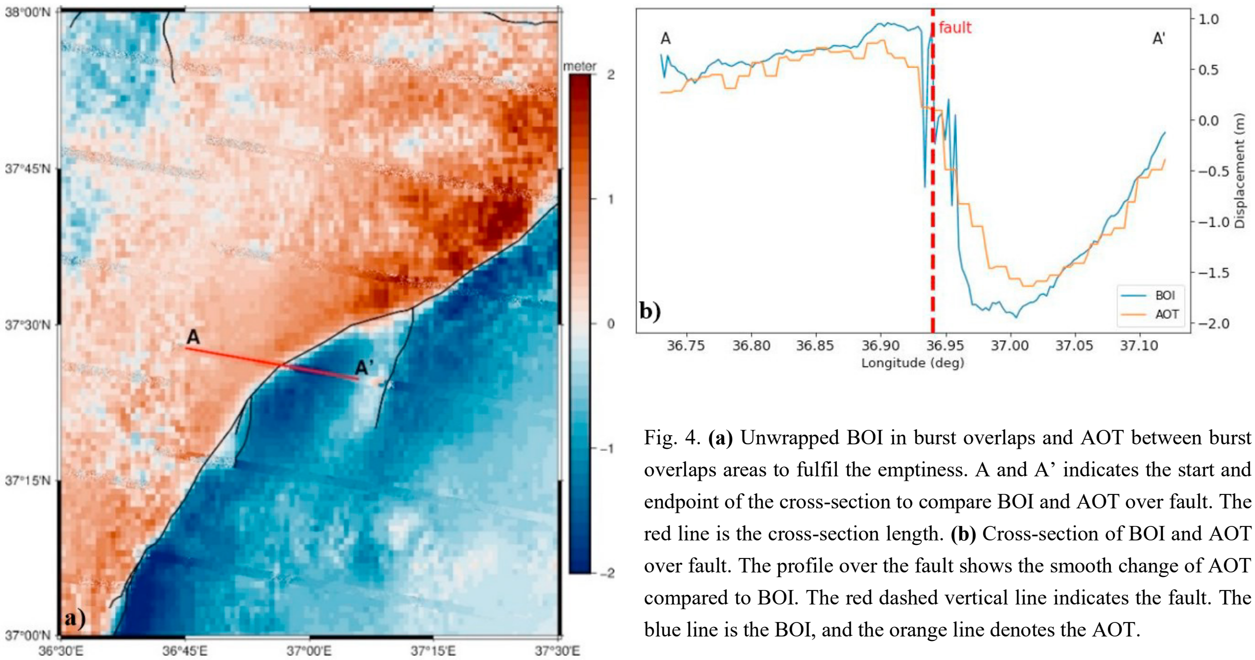

Fig. 4. **(a)** Unwrapped BOI in burst overlaps and AOT between burst overlaps areas to fulfil the emptiness. A and A' indicates the start and endpoint of the cross-section to compare BOI and AOT over fault. The red line is the cross-section length. **(b)** Cross-section of BOI and AOT over fault. The profile over the fault shows the smooth change of AOT compared to BOI. The red dashed vertical line indicates the fault. The blue line is the BOI, and the orange line denotes the AOT.

Acknowledgements

This work was developed in support from The Natural Environment Research Council large grant, "Looking inside the continents from Space" (NE/K010867/1). COMET is the NERC Centre for the Observation and Modelling of Earthquakes, Volcanoes and Tectonics, a partnership between UK Universities and the British Geological Survey. The first author is funded by Republic of Türkiye Ministry of National Education throughout his PhD.

References

[1] E. Hussain, S. Kalaycıoğlu, C. W. D. Milliner, and Z. Çakir, "Preconditioning the 2023 Kahramanmaraş (Türkiye) earthquake disaster," *Nat. Rev. Earth Environ.*, vol. 4, no. 5, pp. 287–289, Apr. 2023, doi: 10.1038/s43017-023-00411-2.

[2] R. Michel, J.-P. Avouac, and J. Taboury, "Measuring ground displacements from SAR amplitude images: Application to the Landers Earthquake," *Geophys. Res. Lett.*, vol. 26, no. 7, pp. 875–878, 1999, doi: 10.1029/1999GL900138.

[3] G. Peltzer, F. Crampé, and G. King, "Evidence of Nonlinear Elasticity of the Crust from the Mw7.6 Manyi (Tibet) Earthquake," *Science*, vol. 286, pp. 272–276, Nov. 1999, doi: 10.1126/science.286.5438.272.

[4] Y. Fialko, M. Simons, and D. Agnew, "The complete (3-D) surface displacement field in the epicentral area of the 1999 MW7.1 Hector Mine Earthquake, California, from space geodetic observations," *Geophys. Res. Lett.*, vol. 28, no. 16, pp. 3063–3066, 2001, doi: 10.1029/2001GL013174.

[5] R. Scheiber and A. Moreira, "Coregistration of Interferometric SAR Images Using Spectral Diversity," *Geosci. Remote Sens. IEEE Trans.*

On, vol. 38, pp. 2179–2191, Oct. 2000, doi: 10.1109/36.868876.

[6] N. B. D. Bechor and H. A. Zebker, “Measuring two-dimensional movements using a single InSAR pair,” *Geophys. Res. Lett.*, vol. 33, no. 16, 2006, doi: 10.1029/2006GL026883.

[7] P. Prats-Iraola, R. Scheiber, L. Marotti, S. Wollstadt, and A. Reigber, “TOPS Interferometry With TerraSAR-X,” *IEEE Trans. Geosci. Remote Sens.*, vol. 50, no. 8, pp. 3179–3188, Aug. 2012, doi: 10.1109/TGRS.2011.2178247.

[8] R. Grandin, E. Klein, M. Métois, and C. Vigny, “Three-dimensional displacement field of the 2015 Mw8.3 Illapel earthquake (Chile) from across- and along-track Sentinel-1 TOPS interferometry,” *Geophys. Res. Lett.*, vol. 43, no. 6, pp. 2552–2561, 2016, doi: 10.1002/2016GL067954.

[9] H. Jiang, G. Feng, T. Wang, and R. Bürgmann, “Toward full exploitation of coherent and incoherent information in Sentinel-1 TOPS data for retrieving surface displacement: Application to the 2016 Kumamoto (Japan) earthquake,” *Geophys. Res. Lett.*, vol. 44, no. 4, pp. 1758–1767, 2017, doi: 10.1002/2016GL072253.

[10] X. Li, S. Jónsson, and Y. Cao, “Interseismic Deformation From Sentinel-1 Burst-Overlap Interferometry: Application to the Southern Dead Sea Fault,” *Geophys. Res. Lett.*, vol. 48, no. 16, p. e2021GL093481, 2021, doi: 10.1029/2021GL093481.

[11] C. W. Chen and H. A. Zebker, “Two-dimensional phase unwrapping with use of statistical models for cost functions in nonlinear optimization,” *J. Opt. Soc. Am. A*, vol. 18, no. 2, p. 338, Feb. 2001, doi: 10.1364/JOSAA.18.000338.

[12] M. Lazecký *et al.*, “LiCSAR: An Automatic InSAR Tool for Measuring and Monitoring Tectonic and Volcanic Activity,” *Remote Sens.*, vol. 12, no. 15, Art. no. 15, Jan. 2020, doi: 10.3390/rs12152430.

[13] Q. Ou, M. Lazecky, C. S. Watson, Y. Maghsoudi, and T. Wright, “3D Displacements and Strain from the 2023 February Turkey Earthquakes, version 1. NERC EDS Centre for Environmental Data.” Mar. 14, 2023. [Online]. Available: doi:10.5285/df93e92a3adc46b9a5c4bd3a547cd242

[14] G. Funning, B. Parsons, T. Wright, J. Jackson, and E. Fielding, “Surface displacements and source parameters of the 2003 Bam (Iran) earthquake from Envisat advanced synthetic aperture radar imagery,” *J. Geophys. Res.*, vol. 110, p. B09406, Sep. 2005, doi: 10.1029/2004JB003338.

[15] S.-H. Yun, H. Zebker, P. Segall, A. Hooper, and M. Poland, “Interferogram formation in the presence of complex and large deformation,” *Geophys. Res. Lett.*, vol. 34, no. 12, 2007, doi: 10.1029/2007GL029745.

[16] T. Wang and S. Jónsson, “Improved SAR Amplitude Image Offset Measurements for Deriving Three-Dimensional Coseismic Displacements,” *IEEE J. Sel. Top. Appl. Earth Obs. Remote Sens.*, vol. 8, no. 7, pp. 3271–3278, Jul. 2015, doi: 10.1109/JSTARS.2014.2387865.

[17] “GAMMA Remote Sensing GAMMA Software Information.” Accessed: Dec. 07, 2023. [Online]. Available: Avaliable online: https://gamma-rs.ch/uploads/media/GAMMA_Software_information.pdf